GEANT4 hadronic cascade models analysis of proton and charged pion transverse momentum spectra from p + Cu and Pb collisions at 3, 8, and 15 GeV/c

Khaled Abdel-Waged,[1,2,*] Nuha Felemban,[1,3] and V. V. Uzhinskii[4]
[1]*Umm Al-Qura University, Faculty of Science, Physics Department, Makkah, P.O. Box 10471, Saudi Arabia*
[2]*Benha University, Faculty of Science, Physics Department, Egypt*
[3]*King Saud University, Faculty of Science, Physics and Astronomy Department, Riyadh, Saudi Arabia*
[4]*CERN, CH-1211, Geneva 23, Switzerland*
(Received 6 December 2010; revised manuscript received 10 June 2011; published 25 July 2011)

We describe how various hadronic cascade models, which are implemented in the GEANT4 toolkit, describe proton and charged pion transverse momentum spectra from p + Cu and Pb collisions at 3, 8, and 15 GeV/c, recently measured in the hadron production (HARP) experiment at CERN. The Binary, ultrarelativistic quantum molecular dynamics (UrQMD) and modified FRITIOF (FTF) hadronic cascade models are chosen for investigation. The first two models are based on limited (Binary) and branched (UrQMD) binary scattering between cascade particles which can be either a baryon or meson, in the three-dimensional space of the nucleus, while the latter (FTF) considers collective interactions between nucleons only, on the plane of impact parameter. It is found that the slow ($p_T \leqslant 0.3$ GeV/c) proton spectra are quite sensitive to the different treatments of cascade pictures, while the fast ($p_T > 0.3$ GeV/c) proton spectra are not strongly affected by the differences between the FTF and UrQMD models. It is also shown that the UrQMD and FTF combined with Binary (FTFB) models could reproduce both proton and charged pion spectra from p + Cu and Pb collisions at 3, 8, and 15 GeV/c with the same accuracy.

DOI: 10.1103/PhysRevC.84.014905 PACS number(s): 24.10.Lx, 24.10.Jv, 25.40.Cm

I. INTRODUCTION

Many hadronic cascade models have been used in macroscopic transport codes, such as GEANT4 [1], FLUKA [2], and CORSIKA [3], to generate nonelastic reactions in macroscopic targets. The motivation was to provide a satisfactory level of description of final-state hadron production for accurate and comprehensive simulations of particle detectors used in modern particle and nuclear physics experiments.

The important implication of the hadronic cascade models is to predict the neutrino fluxes in the accelerator neutrino experiments [4]. In this case one has to know the spectra of produced charged pions in proton-induced reactions on nuclei for the decay chain $\pi^{\mp} \to \mu^{\mp} \to \nu$. Moreover, understanding the neutrino interactions with matter also requires a good description of the secondarily produced particles' (pions and nucleons) interaction with nuclei [5].

In the GEANT4 macroscopic transport code, there are mainly two geometrical methods of simulating N-body collisions within the hadronic cascade models. The first geometrical method assumes a sequential binary cascade developing in the three-dimensional space of the target nucleus. This is the basis of standard intranuclear cascade (INC) [6,7] and hadronic cascade models [8–10]. Even though the standard INC and some hadronic cascade models may present strong similarities, they may differ in how they implement hadronic degrees of freedom. For example, in the ultrarelativistic quantum molecular dynamics (UrQMD) hadronic cascade model [8] many established hadronic resonances including multiparticle production (through the string mechanism) are explicitly propagated and rescatter in phase space, while standard INCs do not include higher hadronic resonances.

On the other hand, some INC models use those sophisticated hadronic models as guidelines to improve the standard INC approach with some of their physics. The GEANT4 Binary cascade model is one such model [11]. It implements a large resonance collision term based on a model similar to that in UrQMD. Multiparticle production through string formation and fragmentation is, unlike UrQMD, not considered, which sets the upper limit of the model applicability in nucleon-induced reactions to ~8 GeV/c incident momentum.

One of the most distinct differences between GEANT4 Binary cascade and UrQMD-INC models is that collisions between participants are not allowed. This may imply that in the course of proton-nucleus (pA) interactions a sequential binary cascade is always developing in a path where the phase-space region is of small densities. This type of cascade picture gives a better description of the high-energy part of the proton spectra for proton-induced reactions at $E \leqslant 800$ MeV, where standard INC codes otherwise often experience limitations in the quality of descriptions [11].

In the second geometrical method, collective cascade occurs in the two-dimensional space of a projected radius vector of nucleons on a plane perpendicular to the momentum of a projectile particle (on a plane of impact parameter) with a cascade power independent of produced particles and defined by Regge constants and the size of the nucleus [12–14]. This method is implemented in the (modified) FRITIOF code of GEANT4, with the abbreviation FTF. The FTF is based on two mechanisms of particle production, namely string formation and string fragmentation. In contrast to the standard FRITIOF model [15], FTF includes (i) kinematical restrictions on the momentum of the (de-)excited string, (ii) collective cascade

*khelwagd@yahoo.com

inspired by the Reggeon theory [16], and (iii) an algorithm for the momentum distributions of the collective cascade particles. These modifications allow the extension of the range of the model applications down to lower momenta, ∼3 GeV/c [17].

In the present paper and in light of recent HARP-CDP proton data induced by proton beams with momentum between 3 and 15 GeV/c [18], we will try to investigate the differences between these models on a purely empirical basis, just by combaring Binary, UrQMD and FTF predictions. The work was done in the framework of the GEANT4 simulation toolkit (version 9.3.p01). Since the UrQMD code is not yet implemented in GEANT4, only the output of the UrQMD calculations is processed in the toolkit [19].

The paper is organized as follows: In Sec. II the basic ingredients of the UrQMD, Binary cascade, and FTF models are defined. In Sec. III, a comparison is made between the model calculations and the HARP-CDP experimental results of proton and charged pion transverse momentum spectra produced in the interactions of 3, 8, and 15 GeV/c protons on Cu and Pb at fixed angles of 30°–40°, 60°–75°, and 105°–125°. Finally, we summarize and conclude this work in Sec. IV.

II. DESCRIPTION OF THE BASIC MODELS

A. The Binary cascade model

The Binary model [11] describes the interactions of protons and neutrons with nuclei as binary collisions between a primary or secondary particle and an individual nucleon of the nucleus, also with associated or direct resonance production and decay. Unlike UrQMD, in case an interaction is allowed, the tracking of the primary ends and the secondaries are treated like the primary. This implies that collision between participants are not considered, limiting the applicability of the model to small participant densities.

Inside the nucleus, particles are propagated in the nuclear field which is approximated by a time-invariant scalar potential, based on the properties of the target nucleus. Outside the nucleus, particles travel along straight-line trajectories. In analogy with the UrQMD model (i) Δ resonances with masses up to 1.95 GeV/c^2 and excited nucleons with masses up to 2.25 GeV/c^2 are taken into account, (ii) the partial and total decay width of a resonance is taken as mass dependent, and (iii) the elastic medium modified angular distributions of the scattered particles, other than nucleon-nucleon scattering, are calculated from the collision term of the relativistic Boltzmann-Uehling-Uhlenbeck (RBUU) equation. The angular distributions for elastic scattering of nucleons are derived from the differential cross sections obtained from the SAID database [20].

B. The UrQMD model

In this section, an outline of the basic ideas of UrQMD is given, which is described in detail in Ref. [8].

The UrQMD model is based on principles that are analogous to the quantum molecular dynamic (QMD) model [21] and the relativistic QMD (RQMD) [9]: the mean field potential applied to hadrons is treated similarly to QMD, while the treatment of the collision term is similar to RQMD. In distinction to our earlier UrQMD calculations [22] where the QMD potential was used, in the present work we will neglect the contribution of the mean field to the reaction dynamics. Therefore, the trajectory of each hadron is straight between two-body collisions, decays, or absorptions.

In the pure cascade calculations of UrQMD, nuclear collisions are assumed to be described by the sum of independent binary hadron-hadron (hh) collisions. Each hh collision is assumed to take place at the distance of closest approach, that is, two particles collide if their distance d_{trans} fulfills the relation

$$d_{\mathrm{trans}} \leqslant \sqrt{\sigma_{\mathrm{tot}}/\pi}, \quad \sigma_{\mathrm{tot}} = \sigma(\sqrt{s}, \mathrm{type}). \tag{1}$$

The total cross section σ_{tot} depends on the c.m. energy $\sqrt{s}$, the species, and quantum number of the particles. The distance d_{trans} is defined as the covariant relative distance between the two colliding particles (in three-dimensional space) as

$$d_{\mathrm{trans}} = \sqrt{(\vec{r}_1 - \vec{r}_2)^2 - \frac{(\vec{r}_1 - \vec{r}_2).(\vec{p}_1 - \vec{p}_2)}{(\vec{p}_1 - \vec{p}_2)^2}}, \tag{2}$$

with $\vec{r}_i$ being the location and $\vec{p}_i$ the momentum in the rest frame of the particles. At the point of closest approach this distance is purely transverse with regard to the relative velocity vector of the particles. During the calculation each particle is checked at the beginning of each time step (in units of time evolution parameter) as to whether it will collide according to criterion (1) within that time step. This procedure assumes that all particles have the same clock. After each binary collision or decay the outgoing particles are checked for further collisions within the respective time steps.

The collision term of the UrQMD treats 55 different baryon species (including nucleon, Δ, Λ, Σ, Ξ, and Ω and their resonances with masses up to 2.25 GeV/c^2) and 32 different meson species (including strange meson resonances with masses up to 1.9 GeV/c^2) as well as their antiparticles and explicit isospin projected states. For excitations with masses >2 GeV/c^2 the string model is used. The exited hadronic states can be produced in either inelastic hh collision, resonance decays, or string decays. All of these hadronic states can propagate and reinteract in phase space.

An analytic expression for the differential cross section of in-medium NN elastic scattering derived from the collision term of the relativistic Boltzmann-Uehling-Uhlenbeck equation [23] is used to determine the scattering angles between the outgoing particles in hh collisions.

A very important aspect of the UrQMD model is an introduction of the formation time and leading prehadron effects. It is assumed that in a high-energy NN collision, two (or more) color-neutral strings are formed, which is stretched between the "colored" ends of each single string. The latter string ends are defined by the space-time coordinates of the constituents, i.e., a diquark (qq) and quark (q) for a "baryonic" string or quark and antiquark for a "mesonic" string. These constituent quarks, diquarks, or antiquarks are denoted as "leading" quarks. These constituent partons are assumed to pick up (almost instantly) an anticolored parton from the vacuum and achieve color neutrality. These color-neutral objects, containing the string ends, are denoted as "leading prehadron." The majority of leading mesons (hadrons) consists mainly of one leading quark and some secondary (di-) quarks.

The time that is needed from the instant of hard collision ($t_0 = 0$) to the production of $q\bar{q}$ or $qq\bar{q}\bar{q}$ pairs from the vacuum ($\tau_p > t_0$) and for the hadronization of the fragments is denoted as formation time (τ_f). The formation time of the ith produced hadron (with energy E_i and longitudinal momentum p_{zi}) is defined as the point in space-time where the quark trajectories of the $q\bar{q}$ pair forming the hadron meet for the first time (the so-called "yo-yo" formation point [24]):

$$\tau_{f,i} = \frac{1}{2}\left(M_s + E_i - p_{zi} - 2\sum_{j=0}^{i-1} p_{zj}\right), \qquad (3)$$

where the string tension κ is $\sim$1 GeV/fm and M_s is the mass of the string. Depending on the hadron species, formation times are on the order of 1–3 fm/c.

For the leading prehadrons, a reduced cross section is adopted according to the constituent quark model:

$$\begin{aligned} \sigma^{\rm pre}_{q,h} &\approx \tfrac{1}{3}\sigma_{B,h} \quad \text{for} \quad \text{baryons}, \\ \sigma^{\rm pre}_{qq,h} &\approx \tfrac{2}{3}\sigma_{B,h} \quad \text{for} \quad \text{baryons}, \\ \sigma^{\rm pre}_{q,h} &\approx \tfrac{1}{2}\sigma_{M,h} \quad \text{for} \quad \text{mesons}, \end{aligned} \qquad (4)$$

during the formation time τ_f and the full hadronic cross section later on. Newly created hadrons without leading quarks of the initial hadron have zero interaction cross section during their formation time.

C. The modified FRITIOF model

The FRITIOF model [15] assumes that the inelastic hh collisions ($a + b \to a' + b'$) result in a transfer of longitudinal momentum between hadrons such that the result is two longitudinally excited strings, where a' and b' are the excited states of initiated hadrons a and b. The model uses the longitudinal excitation as a means of string formation. Each string contains exactly the quarks of one of the incident hadrons. After the string formation, the subsequent string fragmentation follows the Lund fragmentation scheme.

The physical ideas embedded in the fragmentation scheme have been elegantly coded and used in many event generators [8,9,25,26]. However, there are some shortcomings. Firstly, FRITIOF cannot be used for momenta <10 GeV/c. This is due to the fact that no kinematical restrictions on the momentum of the (de-)excited string are set at low energies. Secondly, the FRITIOF model applies the Glauber approach to the evaluation of the number of interacting nuclear nucleons and the sequences of the inelastic nucleon-nucleon collisions, but cascading in the nuclei is not incorporated.

In order to improve the contents of the model for the description of hA interactions, several features are added [12–14].

(i) The collective Reggeon cascading is implemented in the FRITIOF model. It is assumed that a collective Reggeon cascade is developed in the space of impact parameter according to the functional form [12],

$$P(|\vec{b}_i - \vec{b}_j|) = C\exp\big(-|\vec{b}_i - \vec{b}_j|^2/r_c^2\big), \qquad (5)$$

where $\vec{b}_i$ and $\vec{b}_j$ are projections of the radius of ith and jth nucleons on the impact parameter, with $C = 1$ and $r_c = 1.2$ fm. At the first stage, we determine by means of the Glauber approximation, using the DIAGEN algorithm [27], the number of inelastically interacting nucleons, that is, the number of so-called "wounded" nucleons. At the second stage, we consider the noninteracting nucleons, the "spectator" nucleons. It is assumed that a spectator nucleon that is an impact distance $|\vec{b}_i - \vec{b}_j|$ from a hit nucleon can be involved in a Reggeon cascade with the probability of Eq. (5). Such a nucleon can involve another spectator nucleon, and so on.

(ii) The energy and momentum conservation laws are applied to the wounded nucleons; those nucleons which are involved in the first and second stages of the interaction processes. We denote the initial momenta of the wounded nucleons (N) as ($\sum_{i=1}^{N} p_{zi},\ \sum_{i=1}^{N} p_{iT} = 0$). The final momenta ($\sum_{i=1}^{N} p'_{zi},\ \sum_{i=1}^{N} p'_{iT} = 0$) are determined by the algorithm presented in Refs. [14,28], as follows. First we characterize, in the case of two nuclei A and B, the ith wounded nucleon of nucleus A by the variables

$$x_i^+ = \frac{E_i + p_{zi}}{W_A^+} \text{ and } p_{iT}, \qquad (6)$$

and the jth wounded nucleon of the nucleus B by

$$y_j^- = \frac{E_j - q_{zj}}{W_B^-} \text{ and } q_{jT}, \qquad (7)$$

where

$$W_A^+ = \sum_{i=1}^{N_A}(E_i + p_{zi}), \qquad (8)$$

$$W_B^- = \sum_{j=1}^{N_B}(E_j - q_{zj}). \qquad (9)$$

$N_{A(B)}$ is the number of wounded nucleons from $A\,(B)$. Here $E_i(E_j)$ and $p_{zi}(q_{zj})$ are the initial energy and longitudinal momentum of the ith (jth) wounded nucleon. The corresponding total energy and momentum are given by $E^0 = \sum_{i=1}^{N} E_i$ and $p_z^0 = \sum_{i=1}^{N} p_{zi}$, respectively.

Second, we ascribe to each wounded nucleon a momentum $\{y_j'^-(x_i'^+),\ q'_{jT}(p'_{iT})\}$ distributed according to the law:

$$P(y_j'^-, q'_{Tj}) \propto \prod_{j=1}^{N_B} \exp\left(-\frac{q'^2_{Tj}}{\langle q_T^2\rangle}\right) \exp\left[-\frac{(y_j'^- - 1/N_B)^2}{(d/N_B)^2}\right], \qquad (10)$$

under the constraints $\sum_{j=1}^{N_B} q'_{Tj} = 0$ and $\sum_{j=1}^{N_B} y_j'^{-} = 1$. The values of $\langle q_T^2 \rangle = 0.3\,(\mathrm{GeV}/c)^2$ and $d = 0.21$were determined from an analysis of the spectra of particles emitted in hA and AA interactions [29–31]. The final momentum of the ith (jth) wounded nucleon is then obtained in terms of $\{x_i'^{+},\ p'_{iT}\}$ and $\{y_j'^{-},\ q'_{jT}\}$:

$$p'_{zi} = \left(W_A'^{+} x_i'^{+} - \frac{m_{iT}'^{2}}{x_i'^{+} W_A'^{+}} \right) /2, \tag{11}$$

$$q'_{zj} = -\left(W'_B - y_j'^{-} - \frac{\mu_{jT}'^{2}}{y_j'^{-} W_B'^{-}} \right) /2, \tag{12}$$

where $m_{iT}'^{2} = m_i^2 + p_{Ti}'^{2}$, $\mu_{jT}'^{2} = \mu_j^2 + q_{Tj}'^{2}$, and $m_i(\mu_j)$ is the mass of the ith (jth) wounded nucleon from A (B). In the expressions (11) and (12) $W_A'^{+}$ and $W_B'^{-}$ are calculated by applying the energy-momentum conservation:

$$\begin{aligned}\sum_{i=1}^{N_A} E'_i + \sum_{j=1}^{N_B} E'_j &= \frac{W_A'^{+}}{2} + \frac{1}{2W_A'^{+}} \sum_{i=1}^{N_A} \frac{m_{iT}'^{2}}{x_i'^{+}} \\ &\quad + \frac{W_B'^{-}}{2} + \frac{1}{2W_B'^{-}} \sum_{j=1}^{N_B} \frac{\mu_{jT}'^{2}}{y_j'^{-}} \\ &= E_A^0 + E_B^0,\end{aligned} \tag{13}$$

$$\begin{aligned}\sum_{i=1}^{N_A} p'_{zi} + \sum_{j=1}^{N_B} q'_{zj} &= \frac{W_A'^{+}}{2} - \frac{1}{2W_A'^{+}} \sum_{i=1}^{N_A} \frac{m_{iT}'^{2}}{x_i'^{+}} \\ &\quad - \frac{W_B'^{-}}{2} + \frac{1}{2W_B'^{-}} \sum_{j=1}^{N_B} \frac{\mu_{jT}'^{2}}{y_j'^{-}} \\ &= p_{zA}^0 + q_{zB}^0,\end{aligned} \tag{14}$$

and

$$\sum_{i=1}^{N_A} p'_{iT} + \sum_{j=1}^{N_B} q'_{jT} = 0. \tag{15}$$

More explicitly, $W_A'^{+}$ and $W_B'^{-}$ are given by

$$W_A'^{+} = \frac{(W_0^- W_0^+ + \alpha - \beta + \sqrt{\Delta})}{2W_0^-}, \tag{16}$$

$$W_B'^{-} = \frac{(W_0^- W_0^+ - \alpha + \beta + \sqrt{\Delta})}{2W_0^+}, \tag{17}$$

where

$$W_0^+ = \left(E_A^0 + E_B^0\right) + \left(p_{zA}^0 + q_{zB}^0\right),$$
$$W_0^- = \left(E_A^0 + E_B^0\right) - \left(q_{zA}^0 + q_{zB}^0\right),$$

$$\alpha = \sum_{i=1}^{N_A} \frac{m_{iT}'^{2}}{x_i'^{+}}, \quad \beta = \sum_{j=1}^{N_B} \frac{\mu_{jT}'^{2}}{y_j'^{-}},$$

and $\Delta = \left(W_0^- W_0^+\right)^2 + \alpha^2 + \beta^2 - 2W_0^- W_0^+ \alpha - 2W_0^- W_0^+ \beta - 2\alpha\beta$.

(iii) Within the Lund fragmentation scheme, the momentum transfer to a wounded nucleon is given by the probability distribution

$$dw \propto \frac{dP'^{-} dP'^{+}}{P'^{-} P'^{+}}, \tag{18}$$

where $P'^{+} = E' + p'_z$ and $P'^{-} = E' - q'_z$ are the light cone momenta.

In order to take the excitation (increasing mass of the string object) and deexcitation (decreasing mass of the string) processes into account, the variables P'^{-} and P'^{+} are allowed to vary in the intervals

$$[P_i^-, P_j^-],\ \ [P_j^+, P_i^+]. \tag{19}$$

The kinematic restrictions are made by changing condition (19) as follows [17]:

$$[P_i^-, \sqrt{s'_{ij}} - m_j],\ \ [P_j^+, \sqrt{s'_{ij}} - m_i]. \tag{20}$$

Expressions (20) are calculated at $\sqrt{s'_{ij}}=\sqrt{s_{ij}}=E'_i+E'_j=E_i+E_j$, $m'_i = m_i$, and $m'_j = m_j$. The minimal values of P_i^- and P_j^+ are the lower limits in Eq. (20), while the maximal values are achieved when hadrons come to rest in the c.m. frame of NN collisions. After the collision, the masses of the two excited strings should satisfy the kinematical constraint:

$$P^- P^+ \geqslant m'^2 = m^2 + p_x^2 + p_y^2. \tag{21}$$

The two longitudinally excited objects are given an average square of transverse momentum equal to 0.3 GeV$/c^2$.

Formation time is assigned to hadrons from string formation and determined by the Lund fragmentation model [see Eq. (3)]. The concept of prehadrons in the FRITIOF model is, however, different from that used in the UrQMD model: While the production time of prehadrons in the FRITIOF model depends on the energy and momentum of the string fragments, τ_p is set to zero in the UrQMD approach. Moreover, the prehadronic interactions of the color-neutral object between τ_p and τ_f are neglected in FTF [cf. Eq. (4)]. In each scattering event, the individual production and formation time is, thus, assigned for each hadron.

In Fig. 1 we present a comparison of the FTF model calculations without (dashed lines) and with (solid lines) Reggeon cascading for p + Pb collisions at 15 GeV$/c$. As one can see, the effect of cascading is more pronounced in the region of $p_T \approx 0.15 - 0.75$ GeV$/c$ and increases with increasing emission angle.

For a reliable description of p and $\pi^{\pm}$ transverse momentum spectra from p + Cu and Pb collisions at 3, 8, and 15 GeV$/c$, it is necessary to invoke low-energy ($\sqrt{s} \leqslant$ 2.7 GeV) hh final interactions in the FTF model. Thus, in this paper, the FTF model is supplemented with the Binary cascade model. The latter is used to treat low-energy final

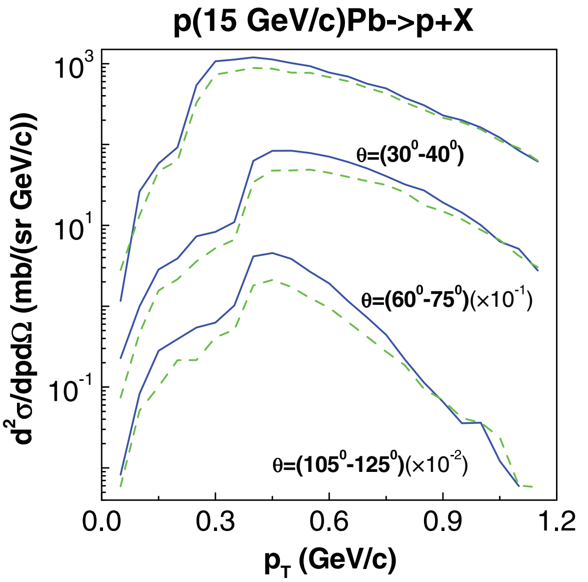

FIG. 1. (Color online) Calculated proton double-differential cross sections as a function of proton transverse momentum (p_T) for $p(15\ \text{GeV}/c)$ + Pb interactions at different angular intervals. Solid lines are the FTF results with Reggeon cascading, while the dashed lines denote the calculations without Reggeon cascading.

interactions which include resonance productions, decays, or absorptions. This extended version we denote as FTFB.

III. NUMERICAL RESULTS

To see the influence of the various physical ingredients of our GEANT4 hadronic cascade models, five types of calculations were done: (i) UrQMD calculations (version 1.3) without mean field and with deactivated *MM* and *MB* collisions, (ii) the same as (i) but with full collision term. (iii) Binary cascade calculations (Binary). (iv) modified FRITIOF calculations (FTF). and (v) FTF combined with Binary calculations (FTFB).

All of the models under study have the following features in common: (a) The initial target nucleus is chosen to be of a Saxon-Wood type, (b) the maximum allowed Fermi momentum is computed according to $P_F = \hbar[3\pi^2\rho(r)]^{1/3}$, where $\rho(r)$ is the nuclear density, and (c) the Pauli principle and the energy-momentum conservation are obeyed in each intranucleon interaction.

In order to ensure that the differences observed in the final results of the GEANT4 hadronic models are regarded as evidence of geometrical cascade effects, the parametrizations of the *pp* and *pn* elastic, inelastic, and total cross sections are checked and found to fit the data well for the momentum range under study.

IV. RESULTS AND DISCUSSIONS

In this section, we systematically apply GEANT4-UrQMD, Binary, and FTF hadronic cascade models to p + Cu and Pb reactions at 3, 8, and 15 GeV/c and investigate the differences between these models by comparing the results obtained by the GEANT4 hadronic cascade models with the recent HARP-CDP data. Only final-state hadrons that stem from the target nuclei are taken into account. In the UrQMD calculations, we exclude generated events with lighter outgoing protons. We performed 50 000 simulations at various impact parameters from 0 to $R + 0.5$ fm, where R is the target radius.

Let us first compare UrQMD (with and without MM and MB collisions) and Binary in the lower parts of the proton spectra (below $p_T \approx 0.2, 0.3.$ and 0.4 GeV/c). These parts are selected to bring out the comparison between both models in the target fragmentation region. Figures 2 and 3 demonstrate that the slow proton spectra of UrQMD calculations with (dash-dotted lines) and without (solid histograms) MM and MB collisions reach a maximum at $p_T = 0.22 \pm 0.05$ GeV/c for all studied interactions and drop rapidly later on. The UrQMD calculations with and without MM and MB collisions coincide at forward angles $\theta = 30^\circ$–40°. However, in the backward angles $\theta \geqslant 60^\circ$–$75^\circ$ calculation without MM and MB collisions (solid histograms) gives lower values at $p_T \approx 0.3 - 0.45$ GeV/c as both the incident momentum and target mass number increase. This directly reflects the fact that MB-binary scattering starts to play a role at $p_T \geqslant 0.3$ GeV/c for the studied reactions. On the other hand, the Binary calculations yield less pronounced peaks, especially for heavier (Pb) target at forward angles. The difference between the UrQMD and Binary peaks is shown to increase when both the target mass number and incident momentum increase. Such behavior can be clearly related to the limiting (binary) cascade picture of Binary compared to UrQMD in the target fragmentation region.

Let us now proceed to the spectra of fast protons. As one can see, the UrQMD predictions with deactivated *MM* and *MB* interactions show a reduced emission of fast protons at $p_T \geqslant 0.3$ GeV/c for all studied interactions. This is due to the fact that proton production in *NN* collisions is forward-backward peaked in the c.m. frame of the colliding nucleons at high momenta. However, the full UrQMD calculation increases the hardening of the proton spectra. This is expected, since nucleons kicked out by the isotropically emitted (in the resonance rest frame) mesons make the p_T spectra harder. The importance of *MB* binary interactions is shown to increase when both the incident momentum and the mass number of the target increase. On the other hand, the Binary tends to underestimate the measured fast proton spectra, even in the range of its applicability (at incident momentum $\leqslant$8 GeV/c). It is interesting to see that Binary (with full collision term) agrees with UrQMD (with deactivated *MM* and *MB* interactions) in the very backward angles ($\theta = 105^\circ$–125°) and in the case of p + Pb interactions at 3 GeV/c, emphasizing too limited binary cascading. This may imply that a better description of fast (and slow) proton spectra can only be achieved in the geometrical binary cascade picture by taking into account a branched-binary cascade with additional MM and MB collisions.

Next, let us look for the effect of a different geometrical cascade picture on slow and fast proton spectra. This is also done in Figs. 2 and 3 by comparing both FTF and UrQMD (without rescattering) with the experimental data. As one can see, at $p_T > 0.3$ GeV/c, FTF generates an excess of fast protons compared to UrQMD, especially when both the mass

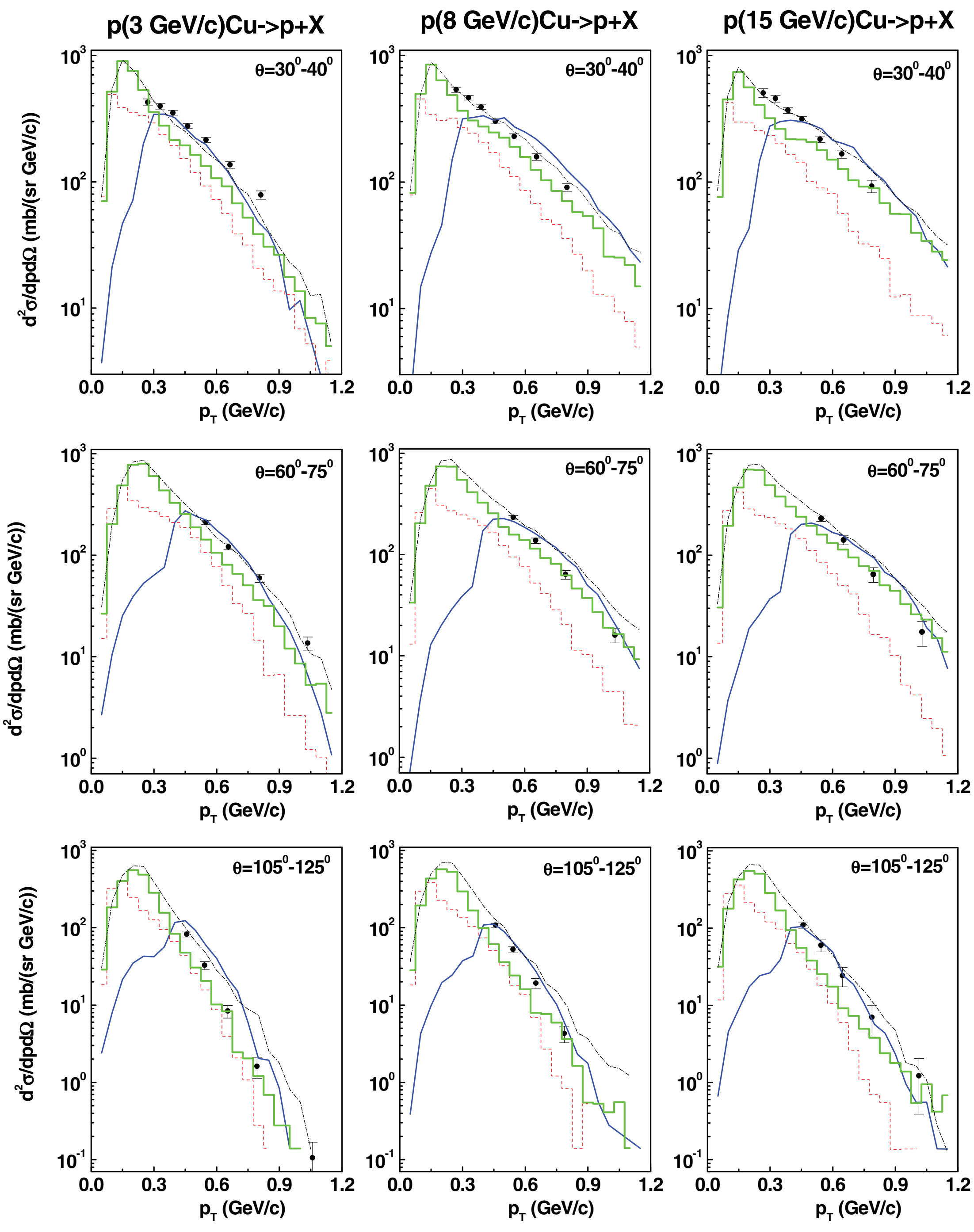

FIG. 2. (Color online) The experimental (error bars) proton double-differential cross sections as a function of proton transverse momentum (p_T) for $p + \mathrm{Cu}$ interactions at 3, 8, and 15 GeV/c at different angular intervals, as compared to GEANT4 hadronic cascade models. Dash-dotted lines and solid histograms denote UrQMD calculations with and without *MM* and *MB* collisions, respectively. The solid lines and dotted histograms denote FTF and Binary cascade calculations, respectively.

number and incident momentum increase. This is caused by the isotropic emission of produced protons [cf. Eq. (10)] in the c.m. frame of the colliding nucleons. Thus one can conclude that the hardening of the fast proton spectra can be achieved by a collective cascade picture without additional *MM* and *MB* rescattering.

It should be noted that the hardening of the proton spectra has also been observed in the Giessen Boltzmann-Uehling-Uhlenbeck (GiBUU) calculations of heavy-ion collisions at 10–20 GeV/A, also due to the isotropic emission of the produced particles in the c.m. frame of a colliding triple [32].

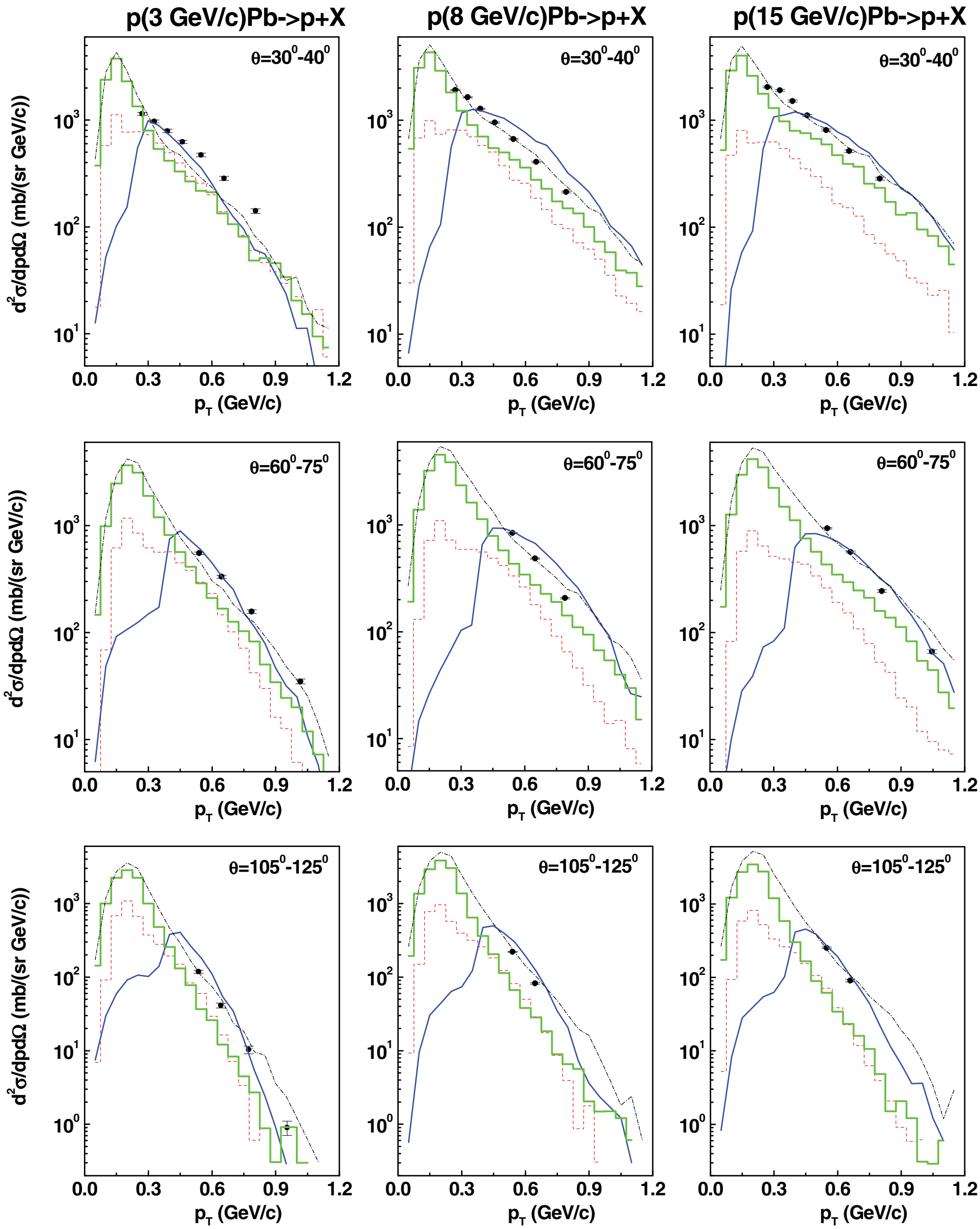

FIG. 3. (Color online) Same as Fig. 2, but for p + Pb interactions.

In general, the FTF calculations are in agreement with both the UrQMD (with full collision term) and the measured fast proton spectra. Only at $p_T > 0.75$ GeV/c, are the UrQMD spectra of fast protons harder than those of FTF. This is again due to the forward-backward peak of binary scattering in the c.m. frame of the colliding nucleons at high momenta.

On the other hand, a systematic difference between FTF and UrQMD (Binary) calculations is observed for p + Cu and Pb interactions at $p_T \leqslant 0.3$GeV/c; FTF is absolutely missing slow proton spectra. The overall reduction of slow particle spectra happens because nucleons emitted from collective cascading are not allowed to rescatter on each other and/or on other particles produced from string decays.

In Figs. 4–9, we study the effect of rescattering on the slow and fast parts of the proton and charged pion spectra. As one can see in Figs. 4 and 5, including Binary into FTF (FTFB) brings calculation into closer agreement with UrQMD for both slow and middle parts ($p_T \approx 0.3 - 0.75$ GeV/c) of the proton spectra at all angular intervals for the studied reactions. In particular, one notices that taking into account

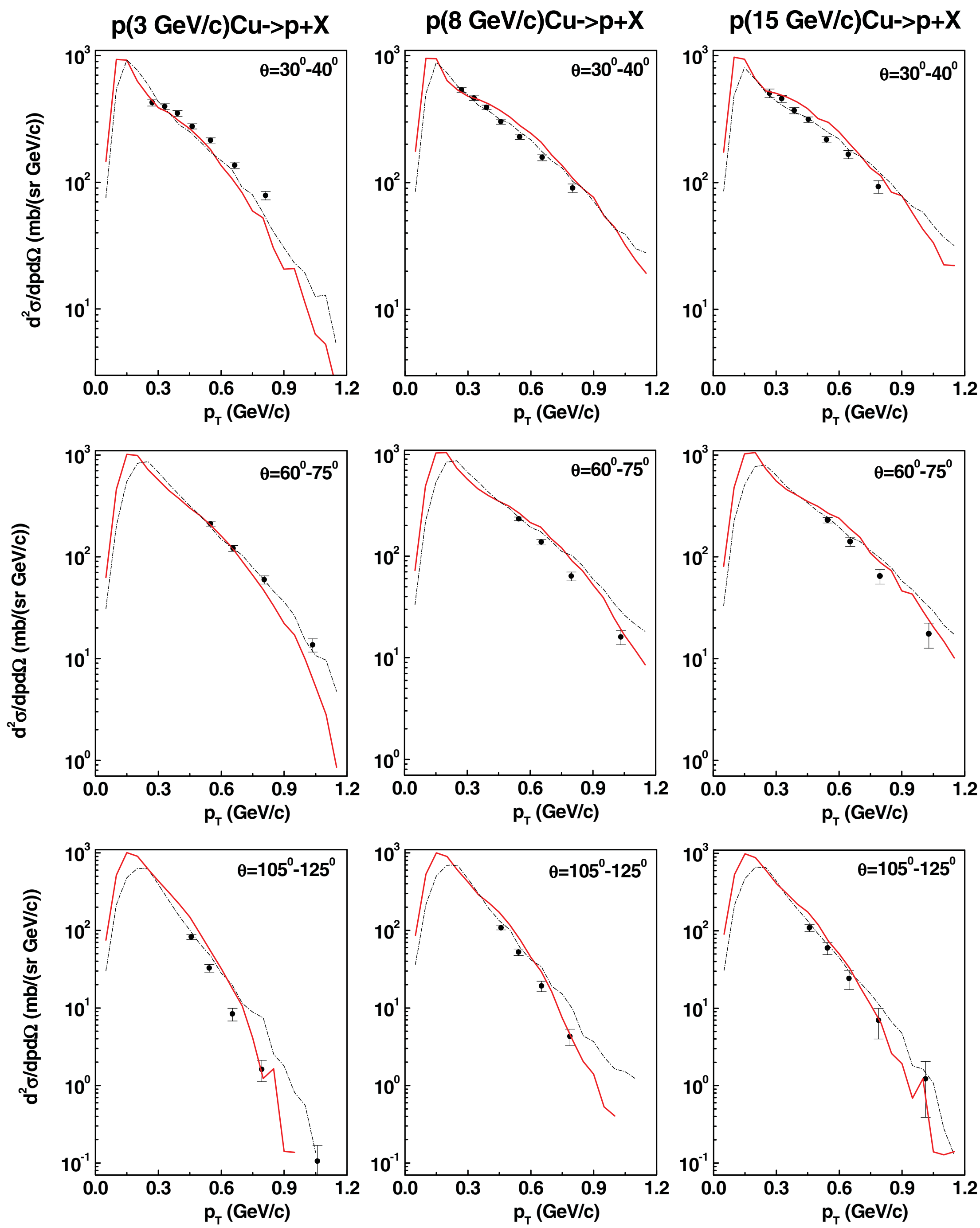

FIG. 4. (Color online) Same as Fig. 2, but here the solid and dash-dotted lines denote UrQMD (full collision term) and FTFB calculations, respectively.

final interactions in FTF strongly increases the slow proton spectra, which results in the formation of peaks, whereas the middle parts of the proton spectra are slightly reduced. This may imply that, in contrast to geometrical binary cascading (cf. Figs. 2 and 3), the rescattering effect in FTF plays an insignificant role for the fast proton spectra.

The effect of rescattering can be even better demonstrated by studying the transverse spectra of the produced charged pions (Figs. 6–9). As one can see, at $p_T \approx 0.25$ GeV$/c$, FTF calculations overestimate the charged pion yields at forward angles $\theta = 30^\circ$–40°. Including rescattering in FTF (solid histograms) reduces the pion yield in good agreement with the data. This is due to the fact that pion absorption via Δ resonance is taken into account in FTFB. Similar to the proton spectra, rescattering does not strongly affect fast pion ($p_T > 0.3$GeV$/c$) spectra.

In general, the UrQMD calculations (dashed histograms) are in agreement with FTFB in the target fragmentation region.

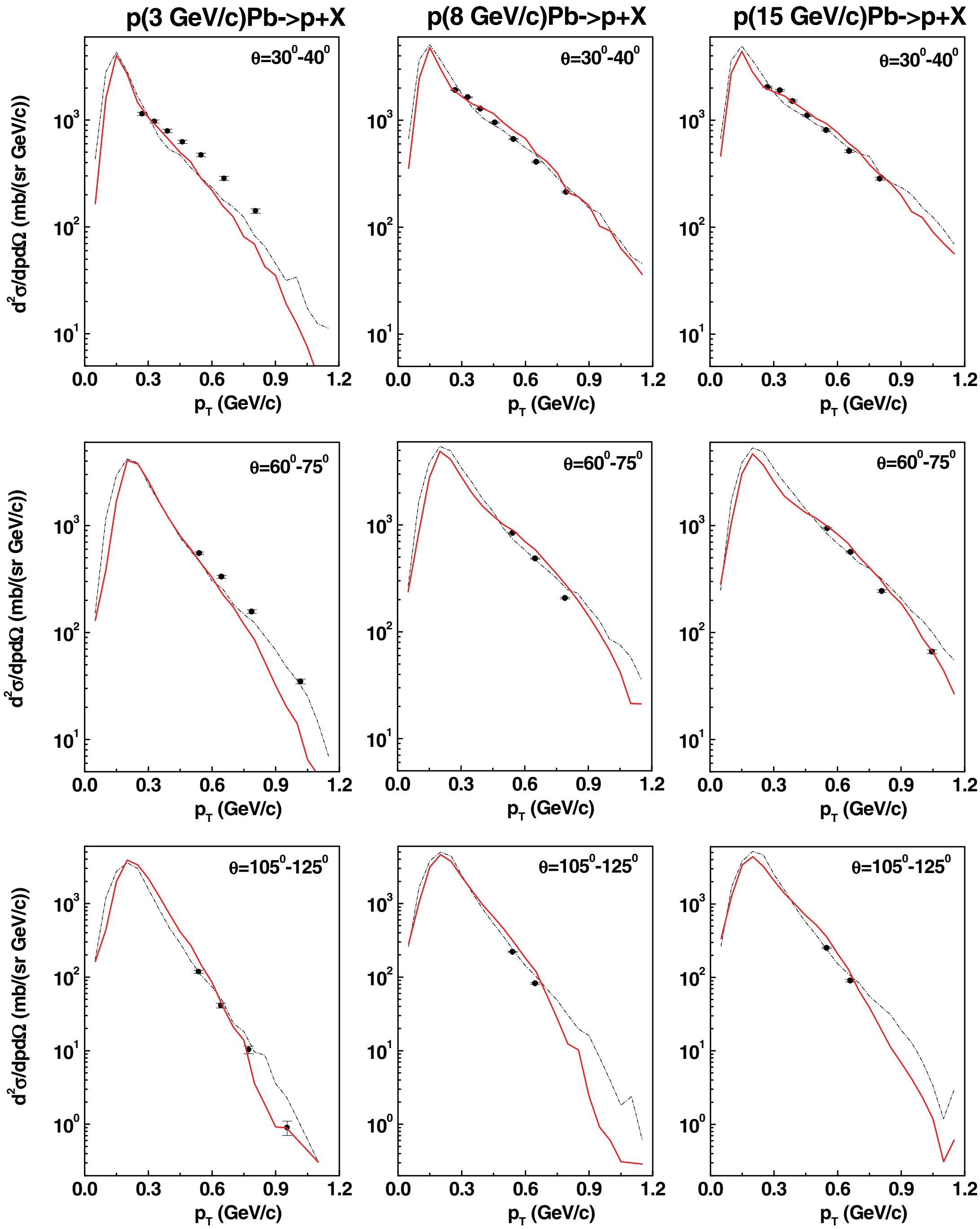

FIG. 5. (Color online) Same as Fig. 4, but for p + Pb interactions.

At $\theta = 30^\circ$–40°, UrQMD, however, shows a reduction of the pion yield at $p_T \approx 0.25$ GeV/c, indicating higher absorption of the Δ resonance. Indeed it is shown in Ref. [33] that the UrQMD model gives higher $\sigma_{N\to NN}$ cross section as a function of $N\Delta$ center of mass energy compared to the data and other transport models. On the other hand, at $p_T > 0.45$ GeV/c, the UrQMD calculations make the pion spectra considerably harder with respect to FTF and in good agreement with the data, especially at lower incident momentum (3 GeV/c). This is caused by the fact that, in UrQMD, pions are produced by two mechanisms of particle production, namely, resonance decays and string fragmentations. At 15 GeV/c, there is almost no difference between UrQMD and FTFB results for the fast pion spectra; they both agree with the corresponding experimental data.

It is worthwhile mentioning that the GiBUU model has been recently compared with the HARP-CDP data [34]. It is shown that a good agreement of the calculated pion spectra from proton-induced reactions with data has been found, except for very forward and backward angles. At the forward angles,

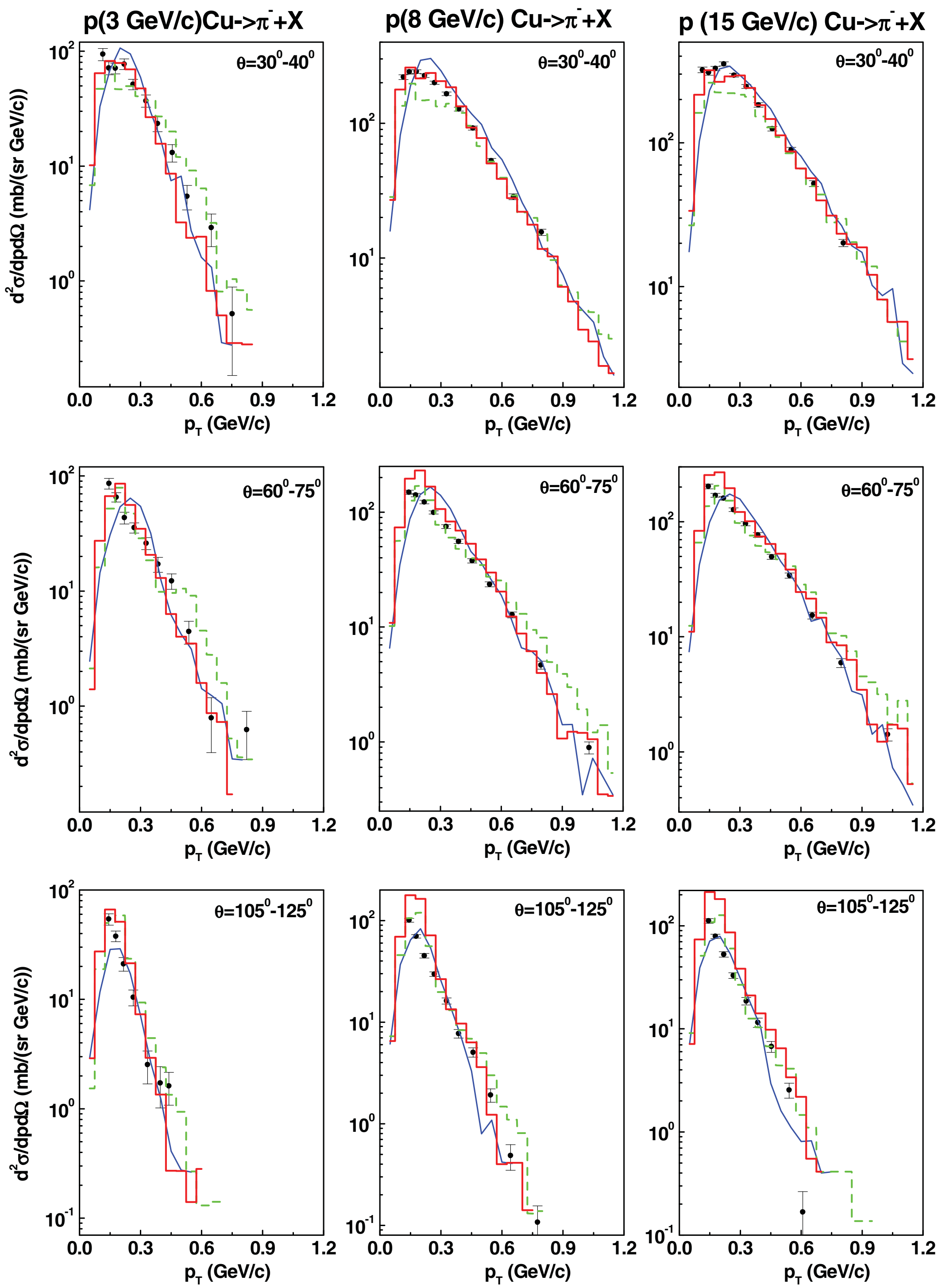

FIG. 6. (Color online) The experimental (error bars) π^--double-differential cross sections as a function of π^- transverse momentum (p_T) for p + Cu interactions at 3, 8, and 15 GeV/c at different angular intervals, as compared to GEANT4 hadronic cascade models. Dash histograms denote UrQMD calculations with *MM* and *MB* interactions. The solid lines and solid histograms denote FTF and FTFB calculations, respectively.

the situation looks similar to the discrepancy of the UrQMD calculations with the measured data as was observed in Figs. 6–9.

Finally, in Fig. 10 we test different prehadronic interaction pictures in comparison to the p and $\pi^\mp$ transverse momentum spectra for p + Pb collisions at 15 GeV/c. The calculations are done within the UrQMD approach, since prehadronic interactions are disregarded by FTF. The default UrQMD results using the simple prehadron concept for the reduced cross sections [Eq. (4)] with the formation time

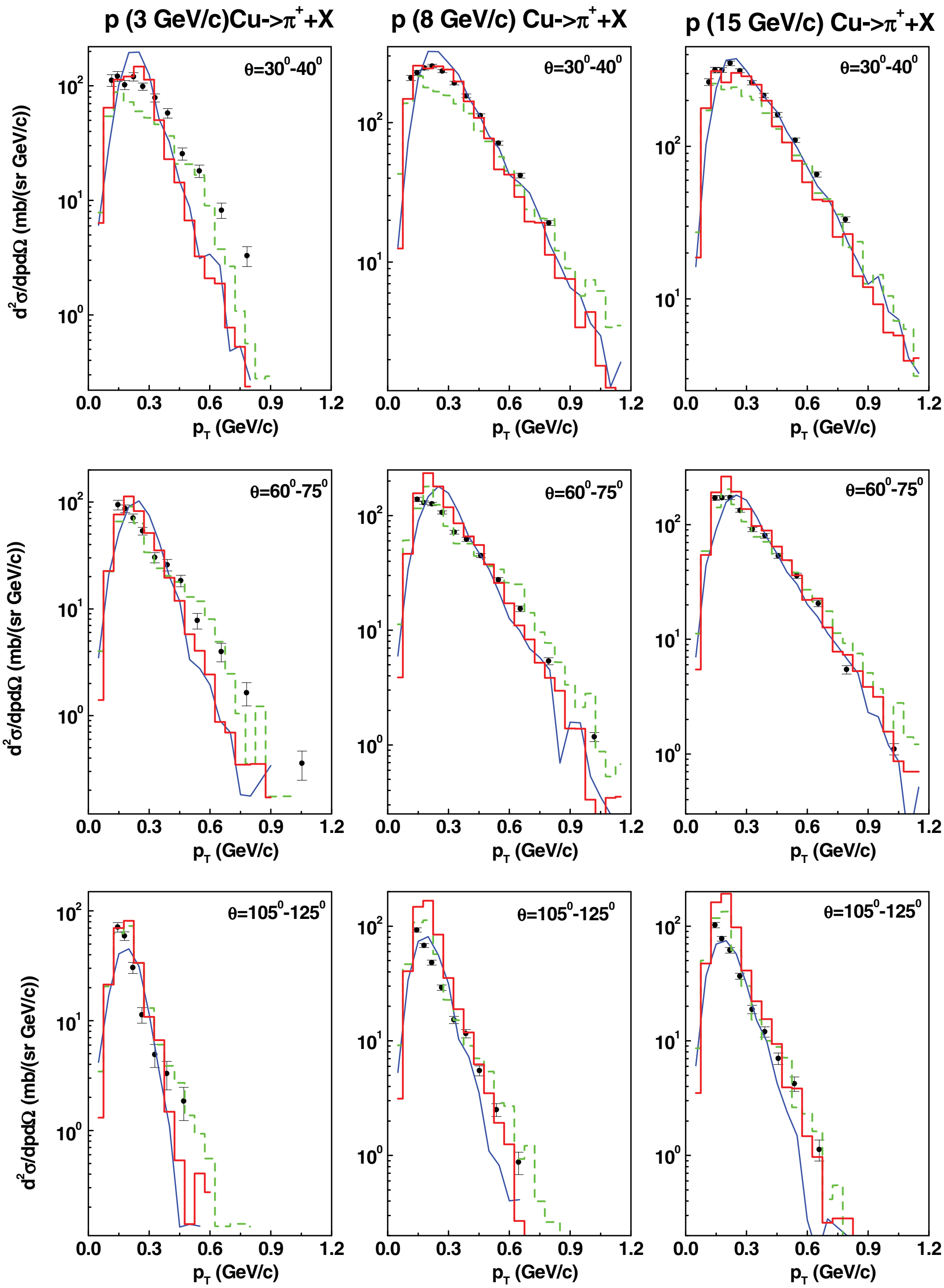

FIG. 7. (Color online) Same as Fig. 6, but for π^+production.

τ_f [Eq. (3)] are shown by the solid lines. We find that, neglecting the prehadronic cross section (σ^{pre}) in the UrQMD calculations leads to dramatic consequences (dashed lines): The p and $\pi^\mp$ transverse momentum spectra are severely underestimated due to the lack of inelastic reactions from leading prehadrons during τ_f. On the other hand, setting σ^{pre} equal to the full hadronic cross section is not sufficient to get the right yield of $\pi^\mp$ observed experimentally in the forward direction ($\theta = 30^\circ$–40°) at $p_T \approx 0.25$ GeV/c (dotted lines).

V. SUMMARY AND CONCLUSIONS

A comparison of the experimental results on the transverse momentum spectra of p + Cu and Pb collisions at 3, 8, and 15 GeV/c is made within the framework of GEANT4 UrQMD,

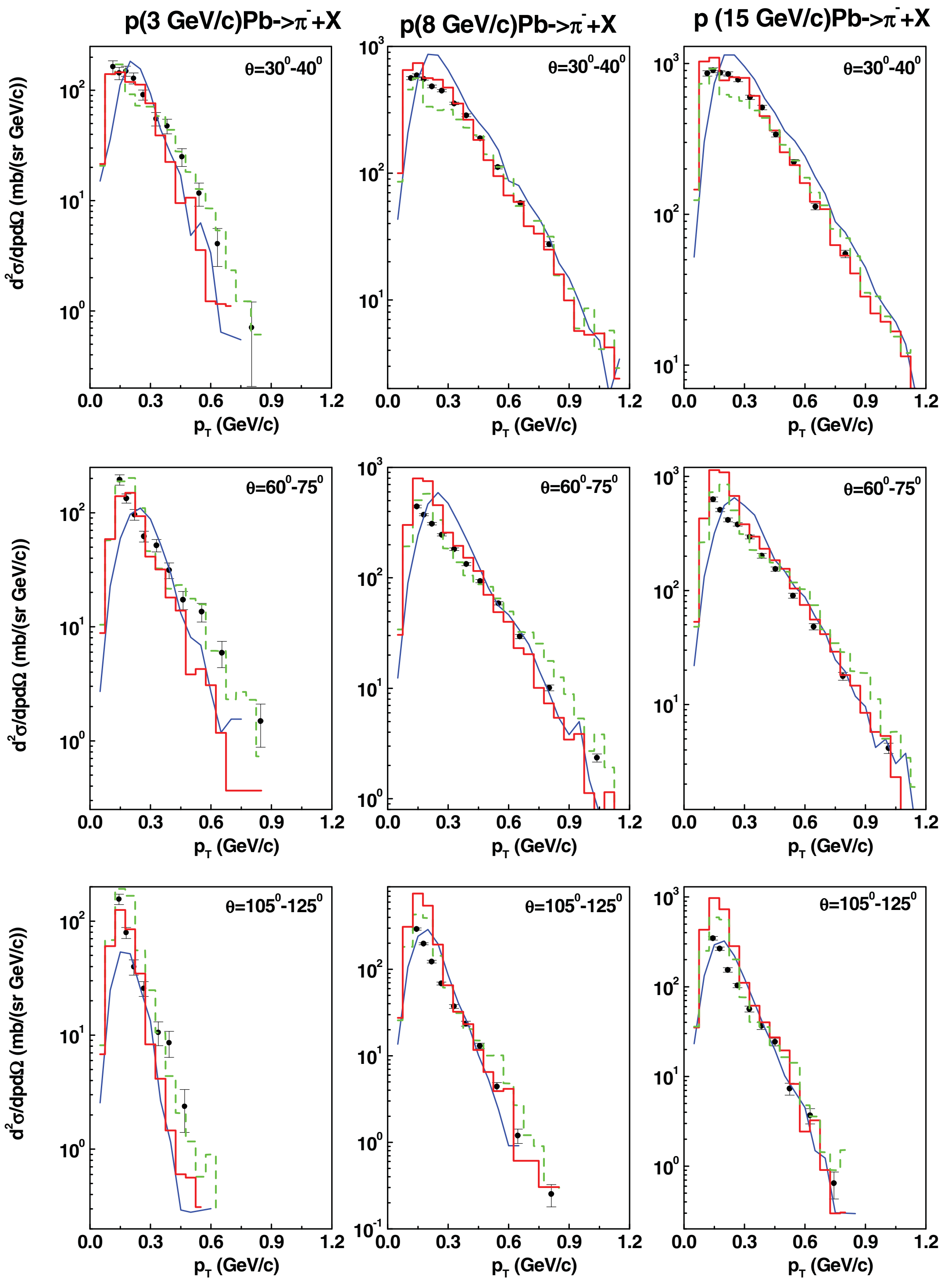

FIG. 8. (Color online) Same as Fig. 6, but for p + Pb interactions.

Binary, and FTF hadronic cascade models. The first two models are based on limited (Binary) and branched (UrQMD) sequential binary hadron-hadron (*hh*) collisions developed in the three-dimensional space of the nucleus, while FTF assumes a collective cascade picture which accounts for a cascade on the plane of impact parameter. In Binary and UrQMD, many well established hadronic resonances are accounted for, while FTF does not include resonance production. String model is adopted in UrQMD and FTF and discarded by Binary. This limits the range of applicability of Binary up to 8 GeV/c. In FTF, kinematical restrictions are made on the momentum of the (de-)excited strings, which extend the range of the model application down to lower momentum $\sim$3 GeV/c; which corresponds to a c.m. energy of $\sqrt{s} =$

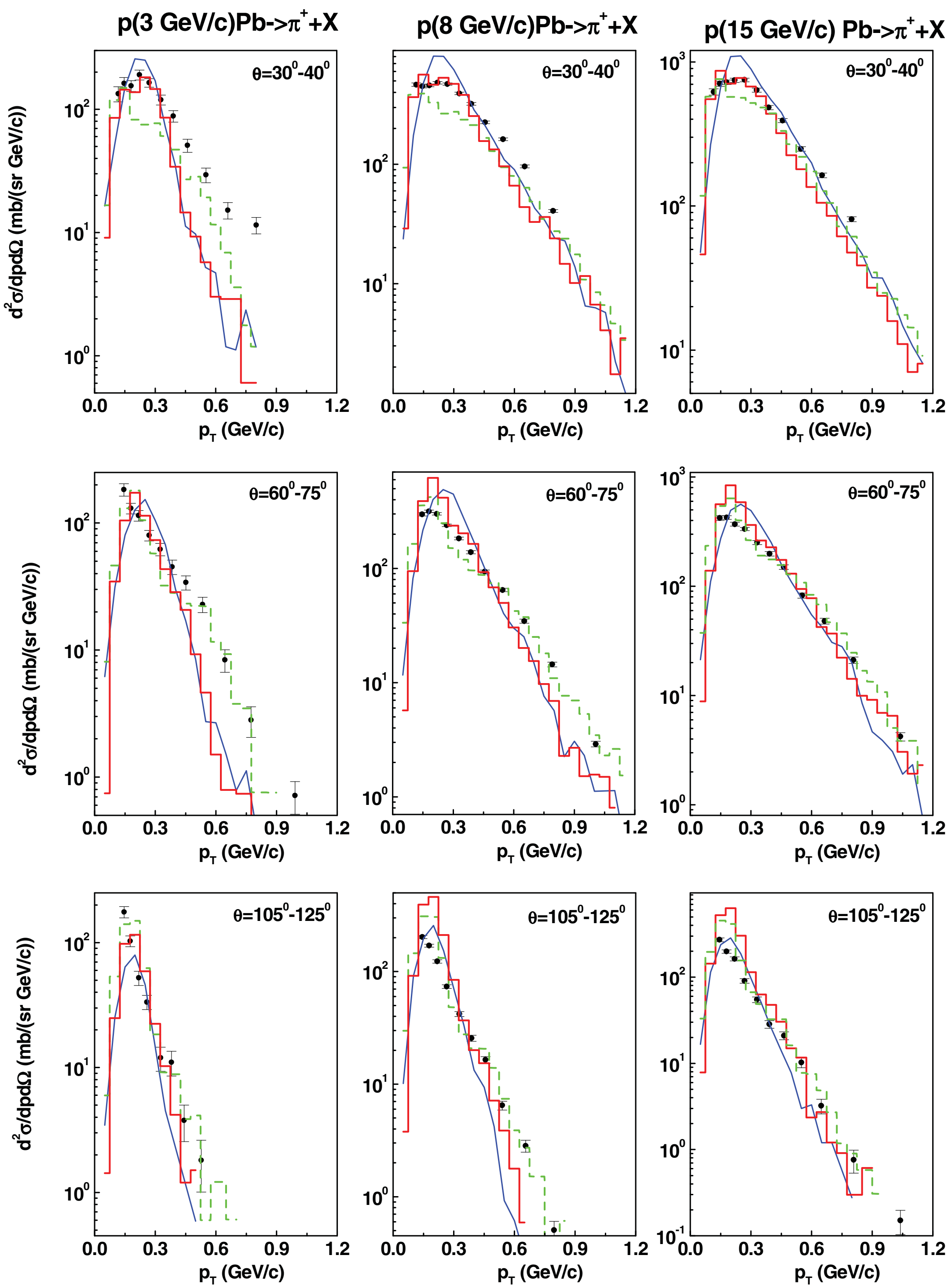

FIG. 9. (Color online) Same as Fig. 6, but for π^+production from p + Pb interactions.

2.7 GeV. We also take into account low-energy ($\sqrt{s} \leqslant$ 2.7 GeV) *hh* final interactions by combining Binary with FTF. This hybrid version is denoted as FTFB. The concept of prehadrons (i.e., produced hadrons interact with some reduced cross section during their formation time) is implemented in UrQMD and discarded by FTF(B). From the calculation results we can draw the following conclusions:

(i) Binary tends to underpredict the measured slow ($p_T \leqslant 0.3$ GeV/c) and fast ($p_T > 0.3$ GeV/c) proton spectra, even in the range of its applicability.
(ii) UrQMD (with or without rescattering) affects slow proton spectra strongly, where a maximum centered around $p_T = 0.22 \mp 0.05$ GeV/c is reached with a fast drop in both sides.

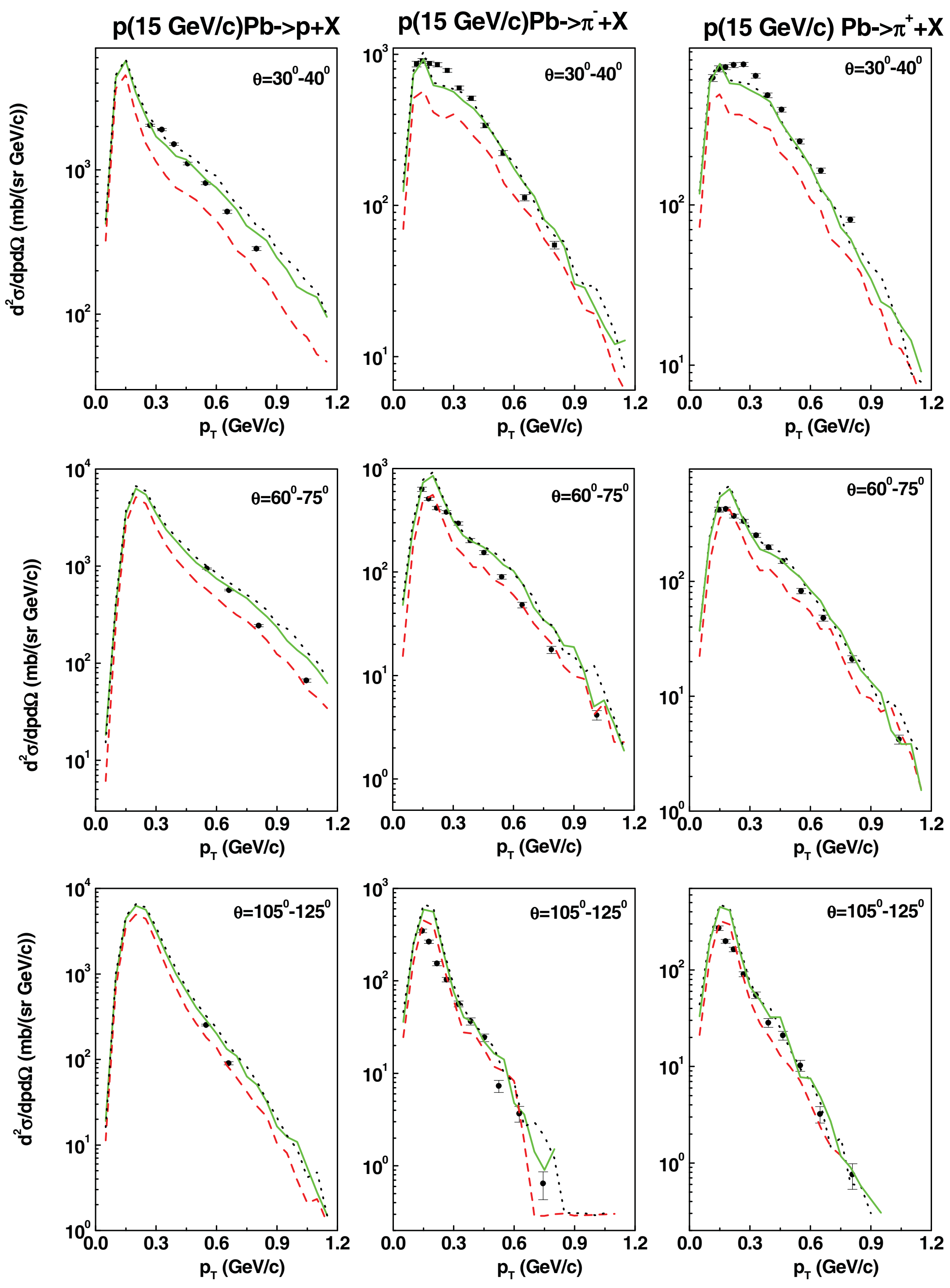

FIG. 10. (Color online) The experimental (error bars) p and $\pi^{\mp}$-transverse momentum spectra for p + Pb collisions at 15 GeV/c. The solid lines show the result of default UrQMD simulation using the constituent quark concept for the prehadronic cross sections [Eq. (4)] and formation time [Eq. (3)]. In the simulation presented by the dashed lines we assume zero prehadronic cross section. The dotted lines represent a simulation where the prehadronic cross section equals the full hadronic cross section.

(iii) The measured fast proton spectra cannot be described by either a limited (Binary) or branched (UrQMD without MM and MB interactions) binary geometrical cascade picture.

(iv) The slopes of the p_T fast spectra of the UrQMD calculation become harder and in better accord with the data by the inclusion of MM and MB interactions; since additional p_T is given to nucleons by the isotropically emitted (in the resonance rest frame) mesons.

(v) Collective cascading (FTF) (without extra *MM* and *MB* interactions) can describe the slopes of the measured p_T fast spectra due to the isotropic emission of the produced protons in the center of mass of colliding nucleons.

(vi) FTFB brings the calculations into closer agreement with UrQMD in the regions of both slow and middle ($p_T \approx 0.3 - 0.75$ GeV/c) parts of the proton spectra.

(vii) At $p_{T\approx}0.25$ GeV/c, UrQMD shows a reduction of the pion yield in the forward direction ($\theta = (30^\circ$–$40^\circ)$; indicating higher absorption via Δ resonance.

(viii) FTFB adequately describes pion absorption seen at $\theta = 30^\circ$–40°.

(ix) Both FTFB and UrQMD are in agreement with each other and the measured fast pion spectra as the incident momentum increases.

(x) Hadron-nucleon cross section modification during the hadron formation time is important for the description of p and $\pi^\mp$-transverse momentum spectra in proton-induced reactions at 3–15 GeV/c.

(xi) Medium effects of MM and MB cross sections should be taken into account in the hadronic microscopic transport models for a better description of $\pi^\mp$-transverse momentum spectra in proton-induced reactions at 3–15 GeV/c.

Our main conclusion of this paper is that, although GEANT4 Binary, UrQMD, and FTF(B) hadronic cascade models are based on completely different physical pictures, the UrQMD and FTF(B) models can describe both proton and charged pion spectra from p + Cu and Pb collisions at 3, 8, and 15 GeV/c with the same accuracy.

ACKNOWLEDGMENTS

This work is supported by the King Abdul-Aziz City for Science and Technology, the National Centre of Mathematics and Physics, Saudi Arabia, Contract No. 31-465. Kh.A.-W. and N.F. thank the members of GEANT4 hadronic group for the hospitality during their visit to CERN. The authors would also like to thank the referee for comments that improved the quality of the paper.

[1] S. Agostinelli *et al.*, Nucl. Instrum. Methods Phys. Res., Sect. A **506**, 250 (2003); J. Allison *et al.*, IEEE Trans. Nucl. Sci. **53**, 270 (2006).

[2] A. Ferrari *et al.*, FLUKA: a multi-particle transport code, CERN 2005-10 (2005); G. Battistoni *et al.*, The FLUKA code: Description and benchmarking, Proceedings of the Hadronic Shower Simulation Workshop 2006, Fermilab 6-8 September 2006, edited by M. Albrow and R. Raja, AIP Conf. Proc. **896**, 31 (2007).

[3] D. Heck *et al.*, CORSIKA: A Monte Carlo Code to Simulate Extensive Air Showers, Forschungszentrum Karlsruhe Report FZKA 6019 (1998); [http://www-ik.fzk.de/corsika/physics_description/corsika_phys.html].

[4] M. Bonesini and A. Guglielmi, Phys. Rep. **433**, 65 (2006).

[5] T. Leitner, L. Alvarez-Ruso, and U. Mosel, Phys. Rev. C **73**, 065502 (2006).

[6] H. Bertini, Phys. Rev. **131**, 1801 (1963).

[7] V. S. Barashenkov, K. K. Gudima, and V. D. Toneev, Acta Phys. Pol. **36**, 415 (1969).

[8] S. A. Bass *et al.*, Prog. Part. Nucl. Phys. **41**, 225 (1998); M. Bleicher *et al.*, J. Phys. G: Nucl. Phys. **25**, 1859 (1999).

[9] H. Sorge, R. Mattiello, A. Jahns, H. Stocker, and W. Greiner, Phys. Lett. B **271**, 37 (1991).

[10] L. Bravina, L. P. Csernai, P. Levai, and D. Strottman, Phys. Rev. C **50**, 2161 (1994).

[11] G. Folger, V. N. Ivanchenko, and J. P. Wellisch, Eur. Phys. J. A **21**, 407 (2004).

[12] Kh. Abdel-Waged and V. V. Uzhinskii, Phys. Atom. Nucl. **60**, 828 (1997).

[13] Kh. Abdel-Waged and V. V. Uzhinskii, J. Phys. G: Nucl. Phys. **24**, 1723 (1998).

[14] M. I. Adamovich *et al.* (EMU01 Collaboration), Z. Phys. A: At. Nucl. **358** (1997).

[15] B. Nillsson-Almquist and E. Stenlund, Comput. Phys. Commun. **43**, 387 (1987).

[16] K. G. Boreskov, A. B. Kaidalov, S. T. Kiselev, and N. Ya. Somorodinskaya, Sov. J. Nucl. Phys. **53**, 356 (1991).

[17] Kh. Abdel-Waged, Phys. Rev. C **59**, 2792 (1999); A. S. Galoyan, G. L. Melkumov, and V. V. Uzhinskii, Phys. Rev. Atom. Nucl. **65**, 1722 (2002).

[18] A. Bolshakova *et al.*, Eur. Phys. J. C **64**, 181 (2009); A. Bolshakova *et al.*, *ibid.* **66**, 57 (2010).

[19] Kh. Abdel-Waged, N. Felemban, and V. V. Uzhinskii, "Enabling comparison of UrQMD with Geant4 hadronic models" CERN LCGAPP 2010-04; [http://sftweb.cern.ch\AAdocuments].

[20] R. A. Arndt, I. I. Strakovsky, and R. L. Workman, Int. J. Mod. Phys. A **18**, 449 (2003).

[21] J. Aichelin, Phys. Rep. **202**, 233 (1991).

[22] Kh. Abdel-Waged, Phys. Rev. C **67**, 064610 (2003); **70**, 014605 (2004); **71**, 044607 (2005); **74**, 034601 (2006).

[23] G. Mao, Z. Li, and Y. Zhuo, Phys. Rev. C **53**, 2933 (1996).

[24] B. Andersson *et al.*, Phys. Rep. **97**, 31 (1983).

[25] Y. Nara, N. Otuka, A. Ohnishi, K. Niita, and S. Chiba, Phys. Rev. C **61**, 024901 (1999).

[26] M. Wagner, A. B. Larionov, and U. Mosel, Phys. Rev. C **71**, 034910 (2005).

[27] S. Yu. Shmakov, V. V. Uzhinskii, and A. M. Zadarozhny, Comput. Phys. Commun. **54**, 125 (1989).

[28] S. Yu. Shmakov, N. V. Slavin, and V. V. Uzhinskii, JINR preprint, E2-88-792, Dubna (1988).

[29] D. Armutlisky *et al.*, Z. Phys. A: At. Nucl. **328**, 455 (1987).

[30] H. N. Agakishiev *et al.*, Sov. J. Nucl. Phys. **56**, 1397 (1993).

[31] A. A. Baldin, Sov. J. Nucl. Phys. **56**, 385 (1993).

[32] A. B. Larionov, O. Buss, K. Gallmeister, and U. Mosel, Phys. Rev. C **76**, 044909 (2007).

[33] Q. Li, Z. Li, S. Soff, M. Bleicher, and H. Stocker, J. Phys. G **32**, 151 (2006).

[34] K. Gallmeister and U. Mosel, Nucl. Phys. A **826**, 151 (2009).